ARTICLE OPEN

Check for updates

A hyper-activatable *CAMK2A* variant associated with intellectual disability causes exaggerated long-term potentiation and learning impairments

Miao Pan[1,2], Pin-Wu Liu[1,3,11], Yukihiro Ozawa[1,11], Fumiko Arima-Yoshida[4], Geyao Dong[5], Masahito Sawahata[5], Daisuke Mori[6,7], Masashi Nagase[4], Hajime Fujii[8], Shuhei Ueda[1,2], Yurie Yabuuchi[1], Xinzi Liu[1,2], Hajime Narita[1,2,9], Ayumu Konno[10], Hirokazu Hirai[10], Norio Ozaki[6], Kiyofumi Yamada[5], Hiroyuki Kidokoro[9], Haruhiko Bito[8], Hiroyuki Mizoguchi[5], Ayako M. Watabe[4], Shin-ichiro Horigane[1,2] and Sayaka Takemoto-Kimura[1,2]✉

Intellectual disability (ID) is a neurodevelopmental disorder (NDD) characterized by impairments in intellectual and adaptive functioning, and is highly co-morbid with other NDDs. Recently, de novo missense variants in the gene, *CAMK2A*, which encodes calcium/calmodulin-dependent protein kinase IIα (CaMKIIα), an abundant neuronal protein crucial for synaptic plasticity, learning and memory, have been implicated in ID. However, the causative impact of these mutations remains underexplored. In this study, we developed a heterozygous knock-in mouse model carrying the most prevalent ID-associated *CAMK2A* de novo missense variant, P212L, as a gain-of-function allele. The knock-in mice exhibited increased autophosphorylation of CaMKIIα, indicative of exuberant kinase activity, and consistently showed dendritic spine abnormalities and exaggerated hippocampal long-term potentiation induced by a subthreshold low-frequency stimulation. Furthermore, a comprehensive behavioral evaluation, including learning and memory tasks, revealed prominent phenotypes recapitulating the complex clinical phenotypes of humans with ID/NDDs harboring the same variant. Taken together, we propose that aberrant enhancement of CaMKIIα signaling by the heterozygous P212L mutation underlies a subset of ID/NDD features. These findings provide new insights into the pathogenesis of ID/NDDs, specifically through the genetic up-shifting of the critical memory regulator, CaMKII. Additionally, the established mouse model, with both construct and face validity, is expected to significantly contribute to the understanding and future therapeutic development of ID/NDDs.

Translational Psychiatry (2025)15:95 ; https://doi.org/10.1038/s41398-025-03316-4

INTRODUCTION

Neurodevelopmental disorders (NDDs) are a group of conditions including autism spectrum disorder (ASD), intellectual disability (ID) attention deficit hyperactivity disorder (ADHD) and developmental coordination disorder (DCD) with onset in the developmental period arising as a consequence of abnormal assembly and wiring of the nervous system [1, 2]. Patients with ID, one of the most common NDDs are characterized by deficits in intellectual and adaptive functions [1, 2]. Recent whole exome sequencing studies have revealed that up to 60% of non-syndromic severe ID cases are associated with de novo pathogenic mutations [3]. Among these, mutations to genes regulating dendritic spine formation and synaptic plasticity have featured prominently [4]. Notably, de novo mutations in *CAMK2A*, encoding calcium (Ca^{2+})/calmodulin (CaM)-dependent protein kinase II (CaMKII), an abundant protein in the postsynaptic density mediating synaptic plasticity, and learning and memory [5–10], has been suggested to be causative for ID [11–14].

Upon synaptic transmission causing depolarization sufficient to trigger Mg^{2+} unblock of NMDA-type glutamate receptors (NMDAR) and opening of voltage-gated calcium channels, Ca^{2+} flows into neurons. This leads to Ca^{2+}/CaM binding to CaMKII, inducing its activation and phosphorylation of downstream substrates as well as autophosphorylation of CaMKII at threonine 286 (T286 in its α-isoform). T286 autophosphorylation enables CaMKII to maintain autonomous kinase activity (autonomy),

[1]Department of Neuroscience, Research Institute of Environmental Medicine, Nagoya University, Furo-cho, Chikusa-ku, Nagoya, Aichi, Japan. [2]Molecular/Cellular Neuroscience, Nagoya University Graduate School of Medicine, 65 Tsurumai-cho, Showa-ku, Nagoya, Aichi, Japan. [3]Graduate School of Medicine, Kyoto University, Yoshida-Konoe-cho, Sakyo-ku, Kyoto, Japan. [4]Institute of Clinical Medicine and Research, Research Center for Medical Sciences, The Jikei University School of Medicine, 163-1 Kashiwashita, Kashiwa, Chiba, Japan. [5]Department of Neuropsychopharmacology and Hospital Pharmacy, Nagoya University Graduate School of Medicine, 65 Tsurumai-cho, Showa-ku, Nagoya, Aichi, Japan. [6]Department of Pathophysiology of Mental Disorders, Nagoya University Graduate School of Medicine, 65 Tsurumai-cho, Showa-ku, Nagoya, Aichi, Japan. [7]Brain and Mind Research Center, Nagoya University, Furo-cho, Chikusa-ku, Nagoya, Aichi, Japan. [8]Department of Neurochemistry, Graduate School of Medicine, The University of Tokyo, 7-3-1, Hongo, Bunkyo-ku, Tokyo, Japan. [9]Department of Pediatrics, Nagoya University Graduate School of Medicine, 65 Tsurumai-cho, Showa-ku, Nagoya, Aichi, Japan. [10]Department of Neurophysiology & Neural Repair, Gunma University Graduate School of Medicine, 3-39-33 Showa-machi, Maebashi, Gunma, Japan. [11]These authors contributed equally: Pin-Wu Liu, Yukihiro Ozawa. ✉email: stakemoto@riem.nagoya-u.ac.jp

Received: 4 October 2024 Revised: 21 February 2025 Accepted: 12 March 2025
Published online: 26 March 2025

allowing the kinase to remain active form even after Ca^{2+} levels decline and Ca^{2+}/CaM binding ceases, an essential event required for synaptic memory [15–17]. Subsequently, the activated and autophosphorylated CaMKII then binds to the NMDAR and facilitates the function of AMPA-type glutamate receptor, thereby playing a critical role in the formation and maintenance of long-term potentiation (LTP), a central machinery underlying learning and memory [7–10, 18]. To elucidate the role of CaMKII in learning and memory in vivo, several mutant mice have been generated using knock-out and knock-in strategies based on substitutions of key residues known to be critical for its kinase regulation [9, 19–24]. These mutant mice exhibit abnormalities in LTP, learning and memory, highlighting the roles of CaMKIIα in these processes. Based on these human and mouse studies, dysregulated CaMKII signaling is possibly a core pathogenic player in the molecular etiology for ID. However, despite our knowledge of CaMKII enzymology, the ID-associated *CAMK2A* mutations cause different amino acid substitutions than those studied so far, and the causative impact of these mutations remains poorly studied.

Among the reported ID-related de novo *CAMK2* mutations [11–14], Pro212Leu (P212L), documented in four unrelated patients, represents the most frequently reported mutation for *CAMK2A*. We previously conducted molecular phenotyping of de novo *CAMK2A* mutations using an optical CaMKIIα FRET sensor, hK2α, which demonstrated that most human ID-associated CaMKII mutations, including P212L, are mild gain-of-function alleles and induce aberrant facilitation of its Ca^{2+}/CaM-dependent kinase activation both in vitro and in neuron [13]. Furthermore, P212L shifted the frequency-dependent CaMKIIα activation curve toward lower stimulation frequencies [13]. The frequency-sensitive CaMKII activation property, previously shown by biochemical and FRET-based experiments [25, 26], is believed to be essential for the integration of synaptic inputs and underlies the roles of CaMKIIα in learning and memory [10, 27]. Yet, it is unknown how this hyper-activatable CaMKIIα enzymatic phenotype translates to specific alterations in neural functions in vivo and whether it is sufficient to cause phenotypes related to ID/NDDs.

In this study, we created a heterozygous (Ht) CaMKIIα P212L knock-in mouse model to elucidate the pathological mechanisms of a human ID stemming from hyper-activatable CaMKIIα variant in vivo. Through this knock-in model, we detected increased autophosphorylation levels at Thr286 of CaMKIIα in synaptosome preparations, as well as enlarged dendritic spines in hippocampal CA1 pyramidal neurons. Consistently, our electrophysiological studies show exaggerated LTP in the hippocampal CA1 region of CaMKIIα P212L mutant mice exposed to a subthreshold low-frequency stimulation, a feature not observed in wild-type hippocampus. Finally, through comprehensive behavioral investigation including multiple learning and memory tasks, we observed behavioral phenotypes reminiscent of, and consistent with clinical phenotypes of humans with this mutation. Thus, we propose that the genetically up-shifting a critical memory regulator, CaMKII, indeed enhances CaMKII signaling in dendritic spines and in neural circuits in vivo, and is sufficient to account for the complex cognitive traits of ID/NDDs in both mice and humans.

MATERIALS AND METHODS

Ethical compliance

All experiments were conducted in accordance with regulations and guidelines for the care and use of experimental animals and approved by the institutional review committees of Nagoya University and of Jikei University School of Medicine.

CaMKIIα P212L mouse construction

CaMKIIα P212L-Ht mice were generated by CRISPR/Cas9 on a C57BL/6J genetic background as previously described [28]. Guide RNAs were designed to target exon 9 (NM_177407.4) of mouse *Camk2a* gene. *Camk2a*-CRISPR RNA (crRNA) (5′- gUGGUCUUCAUCCCAGAACGguuuuagag-cuaugcuguuuug -3′) and trans activating RNA (tracrRNA) (5′- AAACAGC AUAGCAAGUUAAAAUAAGGCUAGUCCGUUAUCAACUUGAAAAAGUGGCAC CGAGUCGGUGCU-3′) were chemically synthesized and purified using polyacrylamide gel electrophoresis (Fasmac). Injection mixtures were prepared following a previously established method [28]. To produce P212L knock-in mice through protein injection, a combination of Cas9 proteins, *Camk2a*-crRNA, tracrRNA, and donor single-strand DNA was prepared in TE buffer, with working concentrations of 100 ng/μl, 0.61 pmol/μl, 0.61 pmol/μl, and 10 ng/μl, respectively. Cas9 proteins were sourced from NEB (M0386S). The donor ssDNA (5′- GGGACACCTGGAT ACCTCTCCCCAGAAGTGCTGAGGAAGGACCCGTACGGGAAGCCCGTGGACCT GTGGGCCTGTGGTAAGTCCAATCCGGAAGCCCTGTTCGTCTCCCAGCCGTCCA GGCCTTTAGCTCCCTCTCCACTTCCCACTACTCCCCTGCGTCATCTCTCCTCTCCT GCTCCTCTCCCTAGGCGTCATCCTGTATATCTTGCTGGTTGGGTAcCCaCtGTTtT GGGAcGAgGACCAGCATCGCCTGTACCAGCAGATCAAAGCTGGTGCCTATGAT GTGAGTGTTGCTCCCCTCTTCTTCTGGGGAGAGCCAGTGGCCTAAGAGGCCAG AGATCTGAGGACACACCACCACTCCTTACCACTGCAGAGGATGGAGTCCAGGG ACGCTCCAAGACTGACCGTCAGAGCCAGGCTATGACCACATGGTGCCTAG -3′) was chemically synthesized by Fasmac. The mixture was then incubated at 37 °C for a minimum of 15 min before being injected into the pronuclei of one-cell-stage zygotes obtained from the C57BL/6J strain (Charles River Laboratories).

For PCR screening of P212L-Ht embryos, genomic DNAs were extracted from mouse tails using proteinase K digestion, followed by a standard phenol extraction method. P212L-Ht embryos were screened using PCR with KOD FX Neo (TOYOBO; KFX-201), and the resulting products were analyzed by electrophoresis in a 2% agarose gel. Primer sequences for gene detection were as follows: 5′- GGATACCTCTCCCCAGAAGTGCTGAG-GAAG -3′ and 5′- GCGGGACACAGCGATCACCTCACACTTGGG -3′. Furthermore, PCR products were further cloned using the Zero Blunt TOPO PCR Cloning Kits (Life Technologies; K270020) and subjected to sequencing analysis, as described previously. Following the establishment of mouse strains, conventional screening was carried out using PCR, followed by Asp718I restriction enzyme digestion of the PCR product to confirm the presence of the targeted allele.

Western blotting

Synaptosome fractionation was performed as described previously [29] with minor modifications. In brief, upon cervical dislocation of the 13-week-old mice, brains were rapidly dissected and placed in liquid nitrogen to prevent protein degradation and dephosphorylation. The frozen brains were then homogenized on ice in cold homogenization buffer containing 0.32 M sucrose, 10 mM HEPES-NaOH (pH 7.4), 1 mM EDTA, protease inhibitor (Nacalai, 04080-11) and phosphatase inhibitor (Roche; 4906845001). The brains were homogenize using the mini cordless grinder (Funakoshi; CG-4A) and stated as "total". Supernatant (S1) was collected after centrifugation of total brain homogenates at 1000× *g* for 10 min at 4 °C, and the subsequent supernatant (S1) centrifuged at 17,000× *g* at 4 °C for 10 min to obtain the synaptosomal supernatant (S2) and crude synaptosome pellet (P2). Protein concentrations were determined using a BCA Protein Assay Kit (TaKaRa; T9300A). Two micrograms of protein was resolved by SDS-PAGE on 10% polyacrylamide gels and transferred to PVDF membranes at 15 V for 12 h at 4 °C in transfer buffer containing 20% MeOH, 25 mM Tris, 192 mM glycine. Then membranes were blocked in 5% skim milk in TBS-T for 30 min and then incubated with different primary antibodies, phospho-CaMKII (T286) (Cell Signaling; 12716, 1:2000), CaMKIIα (Novus Biologicals; NB100-1983, 1:5000) and GAPDH (MBL; M171-3, 1:5000) for 1 h at room temperature. Following the incubation with secondary antibodies labeled with HRP, goat anti-mouse IgG (Abcam; ab97023,1:5000) and goat anti-rabbit IgG (Abcam; ab6721, 1:2000), image acquisition was taken using Bio-Rad ChemiDoc Imaging System and quantification was accomplished using ImageLab software (Bio-Rad). To analyze phospho-CaMKIIα using the phospho-CaMKII antibody, which detect other isoforms of autophosphorylated CaMKII, we quantified the signal intensities of the protein band with approximately 50 kDa.

Kinase assay

Kinase assays were performed as previously described previously [30], with the following minor modifications. Twenty-five micrograms of P2 was subjected to osmotic shock by homogenization in 9 volumes of ice-cold water for 30 min. Subsequently, the protein was mixed with a kinase buffer containing: 50 mM HEPES-NaOH (pH 7.5), 1 mM $MgCl_2$, 1 mM EGTA, 1 mM DTT, 1 mM ATP, protease inhibitor, phosphatase inhibitor, 2 mM $CaCl_2$, and

incubated at 30 °C for 20 s. Control experiments were performed in parallel without addition of 2 mM $CaCl_2$. The autophosphorylation levels of CaMKIIα were detected by the anti-phospho-CaMKIIα (T286) (Cell Signaling; 12716, 1:2000) antibody.

Intracerebroventricular injections

AAV-PHP.eB vectors were produced using the ultracentrifugation method described in a previous paper [31]. Bilateral intracerebroventricular (ICV) injections were performed on postnatal day 0 to label neurons for visualization of dendritic spines, following the method described by Kim et al. [32] with minor modifications. Cryoanesthesia was achieved by placing the mice on a cold metal plate. Using a glass capillary to puncture the head and insert the needle approximately 2 mm deep, perpendicular to the skull surface, approximately 0.8–1.0 mm lateral from the sagittal suture, halfway between lambda and bregma. Then, 2 µl of a mixture of expression vectors comprising AAV-PHP.eB-CBh-FLEx-EGFP (2×10^{10} vg/mouse) and AAV-PHP.eB-CBh-Cre (1×10^{8} vg/mouse) was injected into each lateral ventricle.

Neuronal image acquisition and spine analysis

Mice brains from 8-week-old mice were dissected and post-fixed in 4% PFA containing 0.2% picric acid at 4 °C overnight. Next day, brains were washed with 0.1 M PB and then sectioned at 50 µm thickness by Leica VT1000S vibratome. Images of dendritic spines were acquired with an LSM 710 Laser Scan Microscope (Carl Zeiss) with 63×/1.4 NA oil objective lens. The stack images were analyzed by Imaris software 9.5 (Oxford instruments) semiautomatically. Mushroom-type spines were defined as a spine with a head width greater than 4 µm. All imaging data were analyzed with an investigator blind to the genotypes of mouse brains analyzed.

NeuroTrace staining and brain image acquisition

Sagittal slices of brain samples were incubated with NeuroTrace 640/660 (Molecular Probes, N21483, 1:100) for 40 min at room temperature. After washing with 0.3% PBS-T for one time, slices were washed twice with PBS and then overnight at 4 °C. The following day, a 10 min Hoechst (Invitrogen, H3570, 1:2000) staining procedure was performed. Slice imaging was performed using a BZ-X800 microscope (Keyence) with a 10×/0.45 NA air objective lens.

RNA extraction and RT-qPCR

Total RNAs were extracted from brain tissue homogenates of 13-week-old mice using TRIzol™ Reagent (Invitrogen, 15596-018) and the PureLink RNA Mini Kit (Invitrogen, 12183025). After DNA digestion with DNase I (Invitrogen, 18068015), reverse transcription was performed using the SuperScript IV First-Strand Synthesis System (Invitrogen, 18091050) with 1 µg of total RNA. Real-time quantitative PCR was carried out in a 10 µl reaction containing 2 µl (4 ng) of cDNA using the TB Green® Premix Ex Taq™ II (TaKaRa, RR820S) in a Thermal Cycler TP900 (TaKaRa). The PCR protocol involved an initial denaturation step at 95 °C for 30 s, followed by 45 cycles of denaturation at 95 °C for 5 s, annealing at 62 °C for 30 s, and extension at 72 °C for 30 s. To ensure specificity, melting curve analysis was performed after amplification (15 s at 95 °C, 30 s at 60 °C, and 15 s at 95 °C). Gene expression levels were normalized against the housekeeping gene GAPDH. The real-time PCR primer sequences were as follows: Camk2a, 5′- TGAAGCACCCCAATATCGTC- 3′ and 5′- ACCAATGAC-CACCCCTTGAC -3′, Camk2b, 5′- ACCCACCTTTCTGGGATGAG -3′ and 5′- ACTAAAGGGTAGGGGACTCA -3′, GAPDH, 5′- AACTTTGGCATTGTGGAAGG -3′ and 5′- ACAAGGATGGGGGTTACACA -3′.

Behavioral testing

Mice were group housed in standard laboratory cages in a temperature (22 °C) and humidity (30–70%) controlled condition with 12 h light-dark cycles. Food and water were provided *ad libitum* throughout the experiment except for Touchscreen-based visual discrimination trial and reversal learning trial. Behavior tests was conducted with 10-week-old mice. Three cohorts were used for behavioral testing (Table S1). Behavioral tests were conducted during the light phase (8 A.M. and 8 P.M.) of the 12/12 h light/dark cycle in dedicated testing sound-attenuated rooms. Mice were brought to the waiting area for at least one hour before experimentation. Before behavior tests, all mice were handled for 5 min each day for 3 prior days. Different genotypes were tested in randomized order by investigators blind to the genotypes.

Open field test

Open field tests were performed with an open plastic chamber (40 × 40 × 30 cm) under approximately 100 lux lighting. Each mouse was placed in the corner, locomotor activity was monitored for 20 min using a video-tracking system (TimeOFCR1, O' Hara & Co., Ltd.) to measure spontaneous activity.

Y-maze test

Mice were placed in the center of a Y-maze (three 2.5 cm wide and 38 cm long arms, each set 120° from each other) for 10 min under 80 lux lighting. Arm entries were recorded using an overhead camera. An entry was defined when all four limbs are within the arm and an alternation was defined as a consecutive entry into three different arms. The percentage of alternation was calculated as: the number of alternation/maximum possible alternations (total number of arms entered − 2) × 100.

Elevated plus maze

The elevated plus maze (EPM) involved an apparatus elevated to 50 cm above the floor and consisted of two open arms and two closed arms, each 25 cm long and 5 cm wide. The closed arms had 11.5 cm high walls. Mice were placed in the center area of the EPM under 10 lux lighting. A video-tracking system (TimeEP1, O' Hara & Co., Ltd.) recorded the time spent and entry frequency in each arm for 10 min to assess anxiety-related behavior.

Novel object recognition test

Novel object recognition tests were performed as described previously [33] with minor modifications, as follows. Briefly, testing was performed in a 30 × 30 × 35 field under 12 lux lighting to assess recognition memory. During habituation, mice were allowed to explore the empty field for 10 min for 3 days. After 24 h of habituation, 2 identical objects were placed in the field, and mice were allowed to explore for 10 min. On the test day, one of the familiar objects was replaced with a novel object of a different shape and appearance. Mice were allowed to explore for 5 min. The time spent around each object was measured manually and the discrimination index was calculated as: (time spent on novel object − time spent on familiar object) / total time spent on both objects.

Beam break test

A clear box (44 cm length, 28 cm wide, 18 cm height) was used with a digital counter with an infrared sensor (Brain Science Idea). The test was carried out in the usual feeding environment, the number of beam breaks was monitored every 5 min for 120 min. The locomotor activity was measured by scoring beam breaks.

Three-chamber test

Three-chamber tests were performed using a rectangle cage (60 × 40 cm) that was divided into left, center, and right chamber. Wire cages were placed in the left and right chamber. Behavior was recorded and scored using a video tracking system (TimeCSI, O' Hara & Co., Ltd.). Tests were performed under 10 lux lighting. Mice were first placed in the center chamber and allowed to explore for 12 min with the wire cages empty. After 5 min rest time, a sex-, age-, and strain-matched stimulus mouse was placed in the right wire cage. The test mice were then returned to the center chamber and allowed to explore for 12 min. Social interaction was defined as the time spent around the wire cage.

Rotarod test

Rotarod test (6 cm diameter rod) was used to assess motor coordination. Mice were placed onto the stationary rod for 1 min, followed which the speed of the rotarod was increased from 4–40 rpm over 300 s. After three days of training, mice were subject to a fixed speed mode at 24 rpm for 120 s. The latency at which each mouse fell from the rotating rod was automatically recorded by the detector. The device was cleaned with 75% ethanol solution between mice. Mice underwent four trials a day with 30 min rest each trial on the training day.

Self-grooming test

Self-grooming test is commonly used to assess anxiety. Mice were placed into a new chamber for 20 min under 100 lux lighting. Grooming behaviors included face wiping, scratching and rubbing of the head area including ears, and cleaning of the entire body. After being placed into the chamber

for 10 min, the self-grooming time for each mouse was measured manually.

Contextual- and cued fear conditioning

The fear conditioning test was performed as described previously with minor modifications [34]. Briefly, on Day 1, mouse was placed in a 10 × 17 × 10 cm chamber (shock chamber) illuminated at 200 lux with 50 dB white noise. The conditioned stimulus (CS) was a 30 s, 10 kHz–65 dB tone. During the last 2 s of the CS, a 0.5 mA electrical foot shock was delivered as the unconditioned stimulus (US). Five CS-US stimuli were presented with a 30 s interval after a 120 s habituation. On day 2, the mice underwent a contextual session which was conducted in the same context as the fear conditioning session with no CS and last for 300 s. Cued test was conducted on day 3, in an altered context (10 × 17 × 10 cm, white acrylic chamber). The light condition and white noise were changed to 50 lux and 60 dB. A 180 s CS was provided. Freezing responses were measured using the automated video tracking software TimeFZ2 (O' Hara & Co., Ltd).

Grip strength test

Grip strength was measured using a MK-380M grip strength meter (Muromachi Kikai Co., Ltd). Mice were placed on a 23 × 25 cm grid and gently pulled horizontally backward until they released their grip. A grip strength meter attached to a force sensor measured the peak force formed by the mouse. Forelegs and total limbs grip strengths were measured 5 times for each mouse and the average of the 5 measurements was compared across mouse genotypes.

Barnes Maze Test

The Barnes maze test involves a circular surface with 12 evenly spaced circular holes around its circumference with an escape box under one of these holes. The center of the circumference is illuminated with 540 lux lighting. Visual cues were placed on the walls of quadrants delineated around the circular platform. Latency and time of visits to the holes were recorded using SMART Video Tracking System (Panlab).

Pre-Training trial. Before each trial, the mouse was placed in a white box at the center of the circumference. After a 15 s interval, the box is removed to commence the trial. Each mouse performed 4 trials per day for 5 consecutive days. Each trial was concluded when the mouse entered the escape box, or when 5 min had elapsed from the start of the trial. Mice that entered the escape box voluntarily were allowed to stay inside for 1 min. Mice that failed to enter the escape box were manually guided to the box and stayed for 1 min. Latency was defined as the time taken for the entire body of the mouse to enter the escape box.

Probe trial. One day after the pre-training session, a probe trial was performed with the escape box removed. Mice were allowed to explore the circular surface for 3 min, the time spent in each quadrant was recorded.

Reversal trial. One day after the probe trial, the escape box was relocated diametrically opposite to the original position, and mice were allowed to search the new escape box. Latency was recorded to analyze the cognitive flexibility of mice.

Touchscreen-based visual discrimination task and reversal learning

The protocol used in this study was previously described [35–37]. Mice were subjected to a restriction period where their access to food and water was limited to a 2-h window (17:00–19:00) each day for 1 week prior to the pretraining stage. Mice reached 85–90% of their free-fed body weight within 7 days and during last 3 days' habituation in the restriction phase, mice were offered 20 µl of milk. Next, the task started with 5 stages of pre-training, consisting of habituation, initial touch, must touch, must initiate and punish incorrect, to shape screen-touch behavior. Upon mastering touchscreen operation (≥75% correct responses for 2 consecutive days), mice were proceeded to Normal visual discrimination (VD) trial.

Normal VD trial. Each trial began with the mice touching the nozzle, and then 2 stimuli (marble and fan) were presented simultaneously in the 2 response windows. One stimulus was associated with a liquid reward (20 µl milk), while the other was not. If the mouse touched the correct response, a reward was delivered, while touching the incorrect response resulted in the immediate removal of the stimuli and the initiation of a 5 s time-out period. Following a 20 s inter-trial interval, a correction trial was introduced, where the same stimuli were repeatedly presented in the same location until the mouse made a correct response. Successful completion of the task required achieving a correct response rate of over 80% for 2 consecutive days. Sessions ended either after 1 h or upon completion of 30 trials, whichever came first.

Reversal trial. The reversal learning trial closely resembled the initial acquisition phase of the normal VD trial, with the key difference being the reversal of stimulus contingencies. The stimulus previously linked to a reward now became an incorrect response, while the previously unrewarded stimulus became the correct response.

Electrophysiology

Mice at 8–16 weeks of age were anesthetized deeply with isoflurane by inhalation (5 in 100% O_2), decapitated, and then the brains were quickly removed. Transverse hippocampal slices (400 µm thick) were cut using a LEICA VT 1200S immersed in ice-cold cutting solution containing: 125 mM NaCl, 3 mM KCl, 1.25 mM NaH_2PO_4, 0.1 mM $CaCl_2$, 5 mM $MgSO_4$, 25 mM $NaHCO_3$, 10 mM glucose, and 0.4 mM L-ascorbic acid, and equilibrated with 95% O_2 and 5% CO_2. Slices were maintained for ≥1 h in an interface-type recording chamber (Fine Science Tools or Scientific Systems Design), that was perfused with oxygenated (95% O_2 and 5% CO_2) artificial cerebrospinal fluid (ACSF) consisting of 124 mM NaCl, 4.4 mM KCl, 25 mM $NaHCO_3$, 1.0 mM NaH_2PO_4, 1.2 mM $MgSO_4$, 2.0 mM $CaCl_2$, and 10 mM glucose (flow rate = 1.5–2.5 ml/min) and heated at 30 °C.

Custom-designed bipolar parallel stimulation electrodes (Unique Medical Co., Ltd., TOG211-039a) were placed on a hippocampal slice to stimulate the Schaffer collateral fibers, while a glass pipette with low resistance (~3 MΩ) was placed on the stratum radiatum to record field excitatory postsynaptic potentials (fEPSPs). fEPSPs were recorded with an Axopatch-1D or Multiclamp 700 B amplifier (Molecular Devices), and the signal was digitized with Digidata 1322 or 1550 B and analyzed with pClamp9 or 11 software (Molecular Devices). The stimulus strength was adjusted to evoke fEPSPs with an amplitude of 0.7–1.5 mV. The test pulse (100 s duration) was delivered at 0.05 Hz. To record responses to paired-pulse stimuli, fEPSPs were stabilized for at least 5 min, then paired-pulse stimuli at intervals of 50, 100, and 200 ms were applied at 0.05 Hz. To record synaptic plasticity, fEPSPs were stabilized for 20 min, then a 10 Hz 90 s train was applied, and fEPSPs were recorded for a further 40 min.

The maximal initial slope of fEPSPs was calculated. In paired-pulse stimulation experiments, the ratio of the second fEPSP slope to the first fEPSP slope was calculated. In 10 Hz 90 s stimulation experiments, slopes were normalized to the mean slope of the 20-min baseline and the normalized slopes of three consecutive fEPSPs, corresponding to 1 min, were averaged. To analyze whether changes in fEPSPs were significant, normalized 20-min baseline slopes and normalized slopes of 35–40 min after 10 Hz stimulation were compared. The normalized averages from 35–40 min were compared between the genotypes.

Statistical analyses

Results were expressed as mean ± SEM. Unpaired two-tailed t-tests with Welch's correction, Log-rank (Mantel-Cox) test, One sample t-test, Kolmogorov-Smirnov test, Two-way repeated measures ANOVA test followed by Šídák's multiple comparison tests, Mixed-effects analysis followed by Šídák's multiple comparison tests, Two-way ANOVA test followed by Tukey multiple comparison tests were performed using GraphPad Prism software (GraphPad 10). $p < 0.05$ was statistically significant.

RESULTS

Generation of CaMKIIα P212L heterozygous (Ht) knock-in mice

Individuals harboring a CaMKIIα P212L variant display varying degrees of ID, motor and language developmental delays. Some cases are also co-morbid with ADHD and ASD (Table 1). Pro212 is located in the kinase domain of CaMKIIα close to the T-site, which docks the regulatory segment including Thr286 (Fig. 1A). To investigate the in vivo mechanism underlying ID and NDDs arising from CaMKIIα P212L, we generated CaMKIIα P212L mutant mice using a CRISPR-Cas9 knock-in strategy (Fig. S1A, B). We initially

Table 1. Primary clinical characteristics observed in individuals with a pathogenic variant, P212L, in *CAMK2A*.

	Kury et al. (2017) individual 1	Kury et al. (2017) individual 2	Kury et al. (2017) individual 3	Fujii et al. (2022) individual 4
CAMK2A mutation	Pro212Leu	Pro212Leu	Pro212Leu	Pro212Leu
Sex	male	male	female	female
Mutation origin	de novo	de novo	de novo	de novo
Intellectual disability	severe	mild to severe	moderate	moderate
Language development delay	+	+	+	+
Motor development delay	+	+	+	+
Abnormal behavior	-	hyperactivity, autistic features	aggressive, hyperactive	ASD/ADHD/DCD
Seizures	+	+	-	-

ASD autism spectrum disorder, *ADHD* attention deficit and hyperactivity disorder, *DCD* developmental coordination disorder.

found through breeding of homozygous mutant mice that they exhibited growth failure and premature death before weaning (data not shown). Since heterozygous CaMKIIα P212L mutations have been reported to associate with ID patients, we focused our studies on CaMKIIα P212L Ht mice. The survival rate of CaMKIIα P212L Ht mice is comparable to wild-type (WT) (Fig. S1C); however, Ht mice exhibited some weight gain (Fig. S1D). No overt abnormalities in overall brain structure were observed between WT and Ht mice (Fig. S1E).

Excessive autophosphorylation of CaMKIIα and enlarged dendritic spines in CaMKIIα P212L Ht mice

As we previously showed that the P212L mutation facilitated CaMKIIα activation in vitro and in cultured neurons [13], we investigated the levels of T286 autophosphorylation, an indicator of activated CaMKIIα that is essential for its function [15–17] in synaptic fractions of brain extracts from WT and Ht mice. We also analyzed the total protein levels for CaMKIIα as previous studies indicated disease-associated mutation in CaMKII may affect the amount of protein expression [38, 39]. As shown, the total amount of CaMKIIα was significantly reduced in synaptic fractions of male CaMKIIα P212L Ht mice, compared to male WT mice (Fig. 1B). Interestingly, no such difference was observed in the female mice groups (Fig. 1C). We also assessed mRNA levels for CaMKIIα and found no difference between groups (Fig. S1F). The relative T286 autophosphorylation level of CaMKIIα was significantly increased in male Ht mice compared to WT mice, while no differences were observed between female Ht and WT mice (Fig. 1B, C). These results indicate that P212L mutation enhance CaMKIIα activity per unit in the male Ht mice. The tendency for increased relative T286 autophosphorylation was also observed in the total brain homogenates of male Ht mice but not in female mice (Fig. S1G, H). To investigate the baseline phosphorylation state of downstream substrates, we examined the phosphorylation levels of pS831 GluA1 and pS1303 NR2B, which are putative serine phosphorylation sites for CaMKII. However, no significant changes were observed in synaptosomes (data not shown). These results are not inconsistent with our findings of a decrease in CaMKII protein levels accompanied by an unchanged amount of autophosphorylated CaMKII levels in male Ht mice. To further assess Ca^{2+}-dependent activation of CaMKIIα ex vivo, we incubated synaptosome lysates from those mouse brains with and without Ca^{2+} and examined the T286 autophosphorylation level of CaMKIIα. Ca^{2+} stimulation increased autophosphorylation at T286 in lysates from both WT and Ht mice to levels that were not significantly different, indicating that high-Ca^{2+}-dependent activation of CaMKIIα was not disrupted in Ht mouse brains (Fig. S2).

Given the function of CaMKIIα as a structural regulator in the dendritic spine [5, 6, 8, 40], we next analyzed the spine morphologies. To do this, we performed sparse labeling of pyramidal neurons in the hippocampus CA1 by intracerebroventricular injection of AAV-PHP.eB vectors encoding Cre recombinase and Cre-dependent expression vector for EGFP on postnatal day 0 (P0), at a ratio of 1:200, to clearly visualize dendritic spine morphologies in vivo (Fig. 1D, E). As shown, we observed a significant increase in the dendritic spine head diameters of mushroom-type spines in male CaMKIIα P212L Ht mice compared to male WT mice (Fig. 1F), with no significant difference in the female mice groups (Fig. 1G). Moreover, there was no significant difference in the densities of mushroom-type spines between these groups (Fig. 1H). As CaMKIIα activity is known to increase the size of dendritic spines, our results suggest that enhanced CaMKIIα activity in male Ht mice under their basal brain activity leads to enlarged mushroom-type dendritic spines in hippocampal CA1 neurons.

Exaggerated hippocampal LTP induced by a subthreshold low-frequency stimulation in CaMKIIα P212L Ht mice

Since the expansion of spine size suggests modifications in synaptic plasticity, we next investigated LTP in the hippocampus. Our previous study showed that P212L mutation shifted a frequency-dependent CaMKIIα activation curve toward lower stimulation frequencies in cultured neurons. Specifically, low stimulation frequencies such as 5 and 10 Hz stimuli triggered more pronounced responses in CaMKIIα P212L compared to WT [13]. Therefore, we asked whether CaMKIIα P212L Ht mice exhibit changes after a 90 s 10 Hz stimulation—a frequency that does not induce potent synaptic plasticity in the WT hippocampus. Indeed, we found that male CaMKIIα P212L Ht mice showed significant potentiation in the hippocampal CA1 region at 35—40 min after the 10 Hz train, compared to baseline (M Ht:134.3 ± 13.2%, $n = 9$, $p = 0.03$), whereas this feature was not detected in WT mice (M WT: 91.4 ± 6.6%, $n = 14$, $p = 0.22$) (Fig. 2A). The normalized average of field excitatory postsynaptic potential (fEPSP) slope from 35–40 min was significantly higher in recordings from male CaMKIIα P212L Ht mice compared to WT mice (Fig. 2B). In female CaMKIIα P212L Ht mice, there was a tendency toward potentiation after the 10 Hz train but the difference was not significant (F Ht: 127.1 ± 11.8%, $n = 8$, $p = 0.05$), whereas this tendency was not observed in female WT mice (F WT: 108.6 ± 12.5%, $n = 6$, $p = 0.52$) (Fig. 2A, B). Moreover, we measured the paired-pulse ratio, an indicator of presynaptic release probability, and found no significant differences between the genotypes in male and female mice suggesting no apparent impairment in presynaptic release (Fig. 2C). These results indicated that the male Ht mice displayed LTP in response to lower stimulation frequency. This could possibly be achieved through excessive activation of CaMKIIα P212L, but not the WT by the low-frequency stimulation. These findings suggest that the mistuning of LTP may underlie the cognitive deficits observed in ID patients with the same mutation.

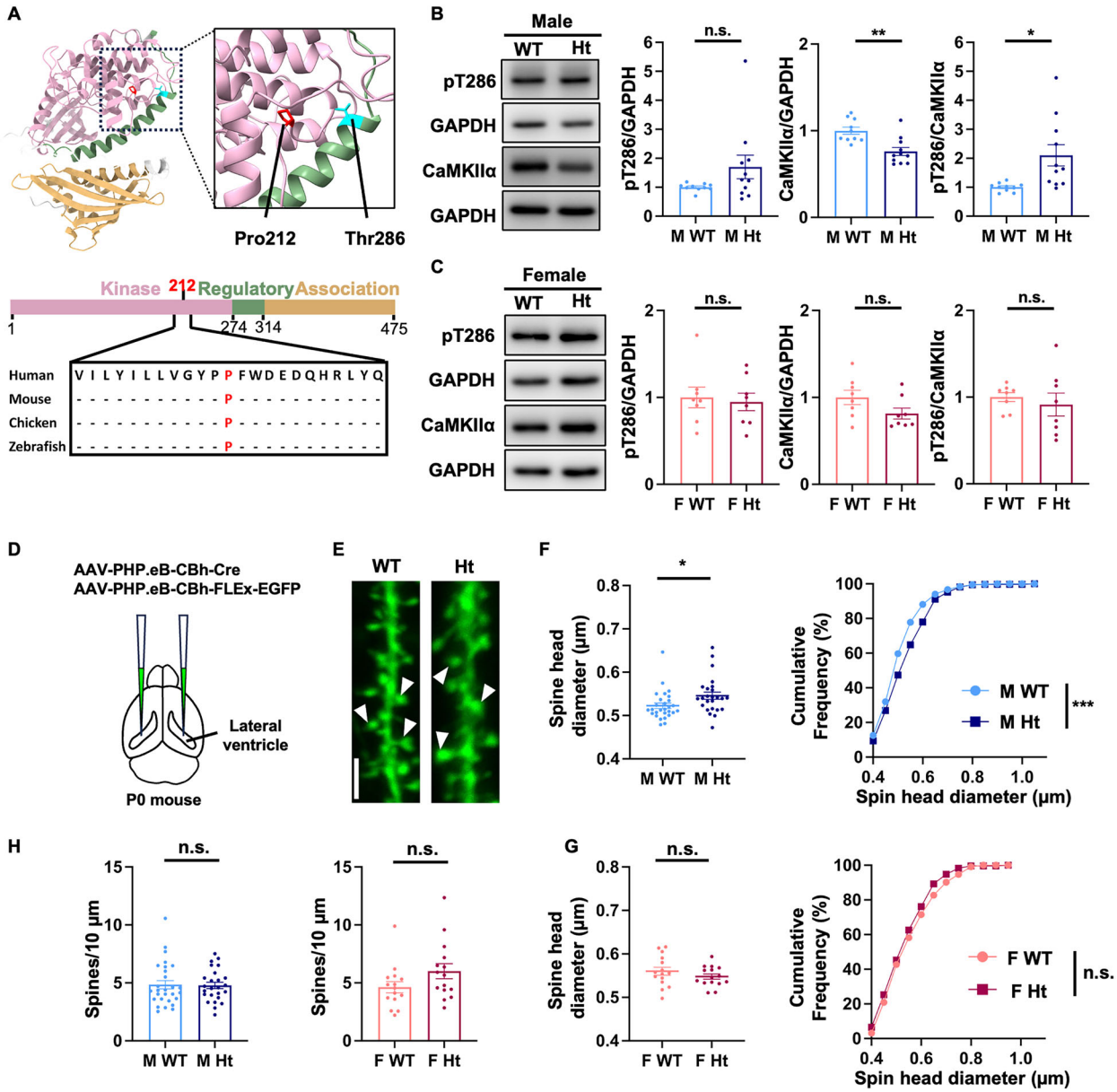

Fig. 1 Increased CaMKIIα kinase activity and enlarged dendritic spine heads of hippocampal neurons in male CaMKIIα P212L Ht mice. **A** Structure of single human CaMKIIα subunit (extracted from a holoenzyme structure: PDB: 3SOA) with the kinase domain (pink), regulatory domain (green), and association domain (straw yellow). Locations of Pro212 and Thr286-autophosphorylation sites are indicated. Multiple sequence alignment of aa193–218 in human CaMKIIα with the indicated animal species. Pro212 is highlighted in red. The alignment was carried out using UniProt. UniProt accession numbers: Human; Q9UQM7, Mouse; P11798, Chicken; A0A8V0YT86, Zebrafish; Q32PV2. **B**, **C** Effects of CaMKIIα P212L mutation on the autophosphorylation levels at T286 and expression levels of CaMKIIα protein. The synaptic fractions were prepared from whole brain homogenates and analyzed by Western blotting. Representative blots are shown in the left panels. (B) Male mice (WT: n = 10, Ht: n = 11), and (**C**) female mice (WT: n = 8, Ht: n = 8) (unpaired Student's t-test). WT: wild-type; Ht: CaMKIIα P212L heterozygous mutant; M: male; F: female. **D** Intracranial injection of AAV-PHP.eB-CBh-Cre and AAV-PHP.eB-CBh-FLEx-EGFP into the cerebral lateral ventricles of neonatal mice to sparsely label pyramidal neurons of CA1 field of the hippocampus. E Representative images of secondary dendrites. The white arrowheads indicate mushroom-shaped dendritic spines. Mushroom spines are defined as spines with a head diameter larger than 0.4 μm. Scale bar, 2 μm. **F**, **G** Mushroom spine head diameters were measured from CaMKIIα P212L neurons versus WT neurons. Average (left panels, unpaired Student's t-test) and cumulative distribution (right panels, Kolmogorov-Smirnov test) of spine diameter are affected in male CaMKIIα P212L mice. **H** Mushroom-type spine density was not affected in CaMKIIα P212L mice. Male: n = 27 spines from 6 WT mice, n = 25 spines from 5 Ht mice. Female: n = 15 spines from 3 WT mice, n = 14 spines from 3 Ht mice (unpaired Student's t-test). Data represent mean ± SEM. *$p < 0.05$, ***$p < 0.001$.

CaMKIIα P212L Ht mice exhibit behavioral phenotypes reminiscent of the clinical phenotypes observed in humans with NDDs

We next investigated behavioral phonotypes of CaMKIIα P212L Ht mice. by conducting a comprehensive behavior test battery. The battery was designed to assess behaviors associated with ID, ASD, ADHD, and DCD described in humans harboring a P212L variant (Table 1) [11, 13].

First, we found that CaMKIIα P212L Ht male mice spent less time in the open arms with longer times in the closed arms in the elevated plus maze (EPM) test, indicating elevated anxiety, while female mice showed no difference between genotypes (Fig. 3A). Locomotor

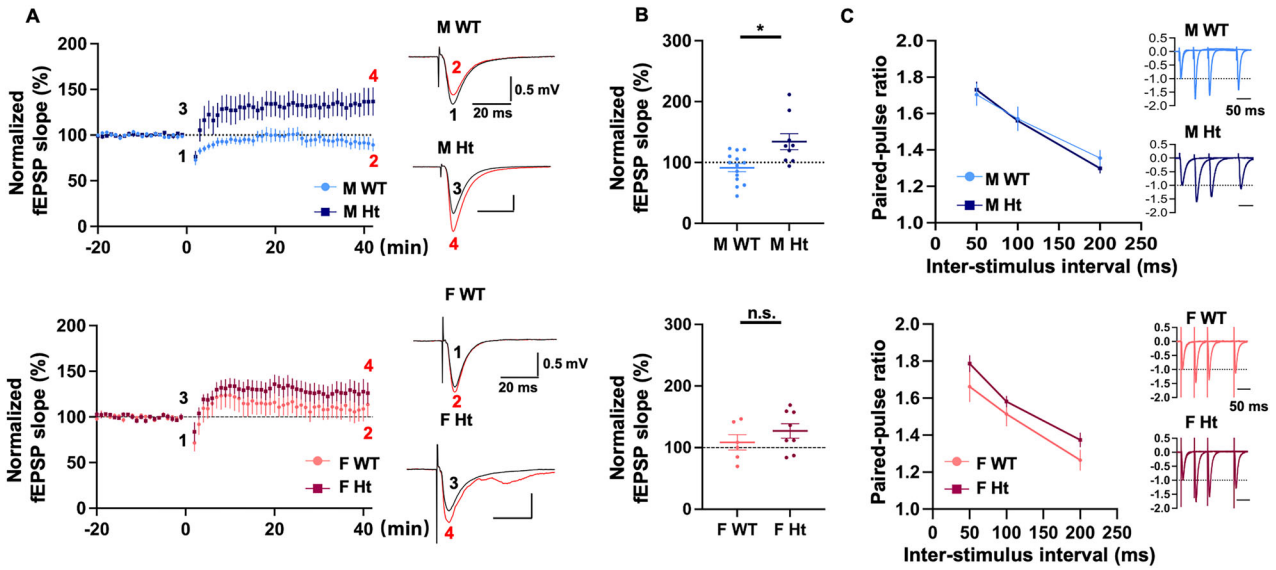

Fig. 2 Aberrant synaptic potentiation in male CaMKIIα P212L Ht mice. A Summary plot of normalized fEPSP slope measurements. Following 20 min of baseline recording, 10 Hz 90 s stimulation was applied. Inset: Sample traces of fEPSPs recorded with hippocampal slices from WT (upper panel) and Ht (lower panel) mice. **B** Plots of normalized fEPSP slope averaged from 35–40 min after 10 Hz stimulation (unpaired Student's t-test). Male: WT; n = 14, Ht; n = 9. Female: WT; n = 6, Ht; n = 8. **C** The paired-pulse ratio of WT and P212L Ht mice at 50, 100, and 200 ms intervals are plotted (two-way repeated measures ANOVA test). Inset: sample traces of fEPSPs recorded in WT (upper panel) and Ht (lower panel) mice. Male: WT; n = 8, Ht; n = 13, Female: WT; n = 9, Ht; n = 7. Data represents mean ± SEM. *$p < 0.05$.

activity tests over an extended period using a beam break test, revealed a significant decrease in total movement distance in both male and female Ht mice compared to WT (Fig. 3B). Furthermore, an open field test showed decreased movement in both male and female Ht mice compared to WT (Fig. S3A). To examine social behavior, we performed three-chamber tests and found that Ht mice spent more time around the stranger mice compared to the WT (Fig. 3C). Motor coordination and learning were assessed using the rotarod test and found that Ht mice exhibited a significantly decreased latency to fall during training in both males and females (day 1–3) and on the test day for females (day 4), indicating impaired motor coordination ability (Fig. 3D). To exclude the possibility of declined muscle strength to affect rotarod test results, we measured grip strength and found no significant difference between groups (Fig. S3D). Next, in a self-grooming test conducted in a novel environment, CaMKIIα P212L Ht male mice showed significantly increased grooming time, suggesting higher anxiety levels (Fig. 3E). We also performed fear conditioning tests, which identified that Ht mice exhibited enhanced fear learning and memory compared to WT mice (Fig. 3F). Additionally, we conducted two learning and memory tests, the Y maze test for working memory and the novel object recognition test for object learning. However, no significant behavioral differences were observed between Ht and WT mice (Fig. S3B, C).

Taken together, we found that Ht mice exhibited elevated anxiety, motor dysfunction, enhanced fear memory, and excessive social behavior, and which are traits reminiscent of ASD- and DCD-related phenotypes diagnosed in humans with a CaMKIIα P212L mutation.

CaMKIIα P212L Ht mice exhibit impairments in spatial and visually guided learning and memory

We next conducted two additional learning and memory tasks to specifically assess the effects of the CaMKIIα P212L mutation on higher cognitive behaviors. We first assessed spatial learning and memory using the Barnes maze test in which the contribution of CaMKII has been well demonstrated compare to other learning types [20, 22] (Fig. 4A). During the training period, male Ht mice showed learning delays on the first and second days but showed improvement thereafter. The same tests conducted using female Ht mice exhibited no significant differences (Fig. 4B). In the following probe trial, all mice spent over a chance level (25%) of their time in the quarter area where the escape hole was located during the training trial, suggesting that the capacity for Ht mice to form spatial memory was not significantly different from WT mice (Fig. 4C). In the subsequent reversal trial, female Ht mice required a longer time to find the new escape hole compared to the female WT mice, whereas male Ht mice showed no significant difference (Fig. 4D). It is worth noting that since only a single session was used in the reversal trial, the results likely reflect the initial response related to cognitive flexibility and may not fully represent the capacity for reversal learning, which is a limitation of our study.

To further explore learning disability in Ht mice, we conducted touchscreen-based visual discrimination (VD) task that evaluate learning without requiring long distance movement, such as with the Barnes maze. We were motivated to carry out this test given that patients with ID harboring CaMKIIα P212L variant showed learning difficulties, particularly with complex reading and writing. The task comprised three trials: a pre-training trial, a normal VD trial, and a reversal trial (Fig. 5A). In the pre-training trial in which mice learned to obtain a reward by poking the screen, no differences were observed between Ht and WT mice in the number of total normal correct trials and days to achieve the goal (Fig. 5B). In the normal VD trial, the mice were presented with two different visual stimuli on the screen, and each mouse needed to touch the correct stimuli to obtain a reward. In this trial, male CaMKIIα P212L Ht mice took significantly more days to achieve the learning goal compared to male WT mice; meanwhile, there were no significant differences in female mice (Fig. 5C), similar to the findings from the Barnes maze test (Fig. 4). In the subsequent reversal trial, mice were presented with the same pair of visual stimuli, but with a reversed reward pairing. In this trial, CaMKIIα P212L Ht male mice exhibited a tendency to take longer and required more correct trials to achieve the learning goal than WT mice (Fig. 5D), whereas there was no significant difference in female Ht mice. Taken together, the results of the Barnes maze test and VD test indicate that male CaMKIIα P212L Ht mice have learning deficits, considered as a trait relate to ID phenotype. Notably, learning disabilities in spatial and visually guided learning

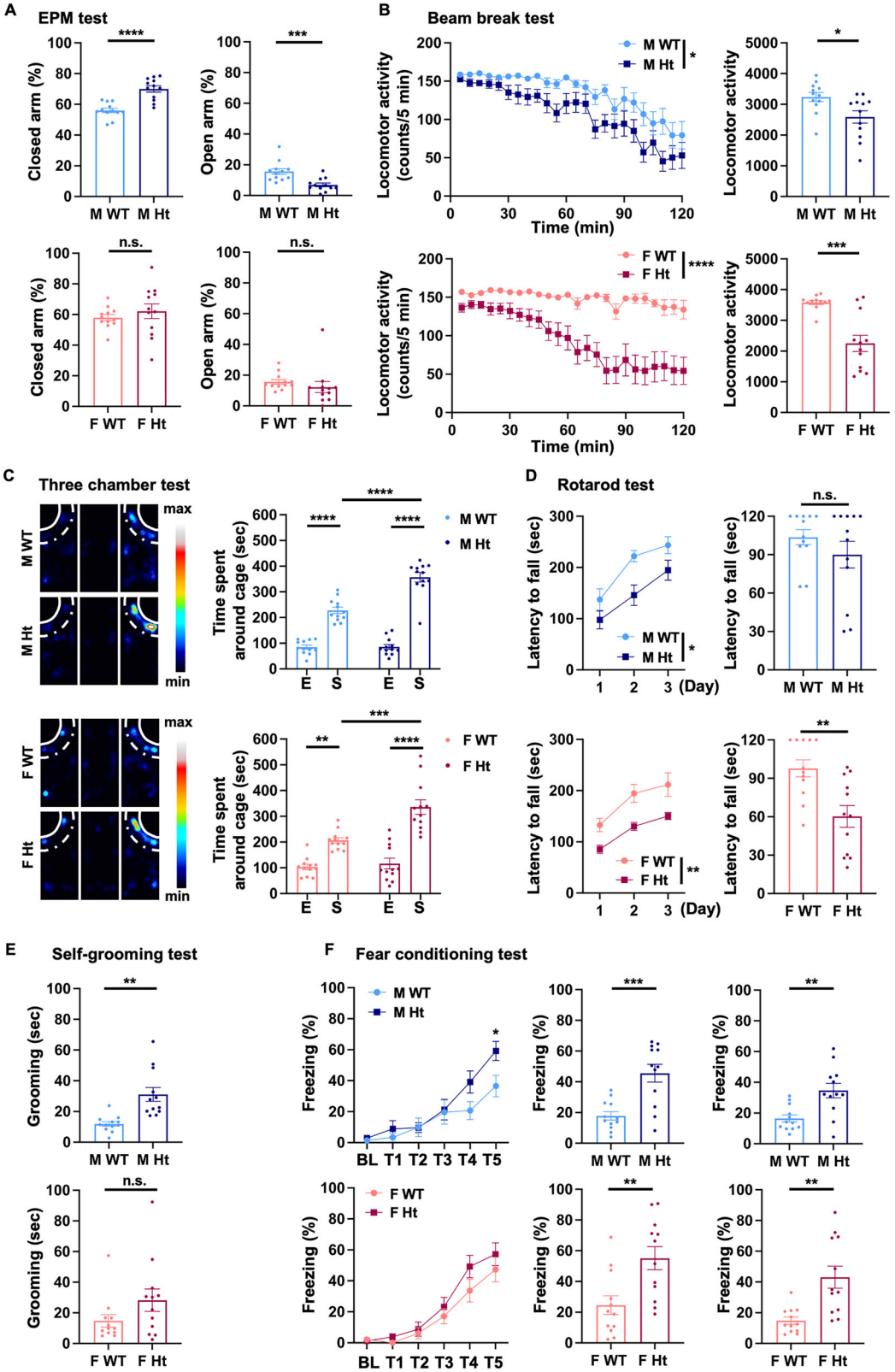

tests of Ht mice are in the opposite direction of enhanced fear memory, showing genetically up-shifting a critical synaptic memory regulator, CaMKII, does not induce a generalized enhancement of learning and memory, but rather induces a complex phenotype consistent with ID/NDDs related cognitive disability.

DISCUSSION

In this study, we generated and characterized a CaMKIIα P212L Ht knock-in mouse model to elucidate the pathological mechanisms for ID and other NDDs arising from a genetic mutation in CaMKIIα. We observed increased levels of CaMKIIα T286 autophosphorylation and consistently enlarged spine morphology in male CaMKIIα P212L Ht

Fig. 3 CaMKIIα P212L Ht mice display ASD- and DCD-related behavioral abnormalities in a comprehensive behavior test battery. A Male CaMKIIα P212L mice show anxiety-like behavior (unpaired Student's t-test). **B** Assessment of spontaneous locomotor activity with a beam break test. A series of beam break counts in 5 min bins are shown in the left panels (two-way repeated measures ANOVA test). Total beam breaks among the 2 h are shown in the right panels (unpaired Student's t-test). **C** Aberrant social behavior in CaMKIIα P212L mice. An empty cage, "E", was placed on the left side, and a stranger mouse, "S", was placed on the right side of the three chambers. Representative heatmap images on the social approach are shown in the left panels. Time spent around the cage is shown in the right panels (two-way ANOVA test, Tukey post hoc test). **D** Motor coordination was affected in CaMKIIα P212L mice. The time for mice to fall off the rod during the three-day training period on the accelerated rotarod test (4–40 rpm, 300 s) is shown in the left panels (two-way repeated measures ANOVA test). The time for mice to fall off the rod on the fixed speed rotarod test (24 rpm, 120 s) on the fourth day is shown in the right panels (unpaired Student's t-test). **E** CaMKIIα P212L mice display an elevated anxiety level in the self-grooming test (unpaired Student's t-test). **F** CaMKIIα P212L mice exhibit enhanced fear memory (two-way repeated measures ANOVA, Šídák post hoc test). Contextual fear memory is shown in the middle panels (unpaired Student's t-test), and cued fear memory is shown in the right panels (unpaired Student's t-test). Male: WT; n = 12, Ht; n = 12, Female: WT; n = 12, Ht; n = 12. Data represents mean ± SEM. *$p < 0.05$, **$p < 0.01$, ***$p < 0.001$, ****$p < 0.0001$.

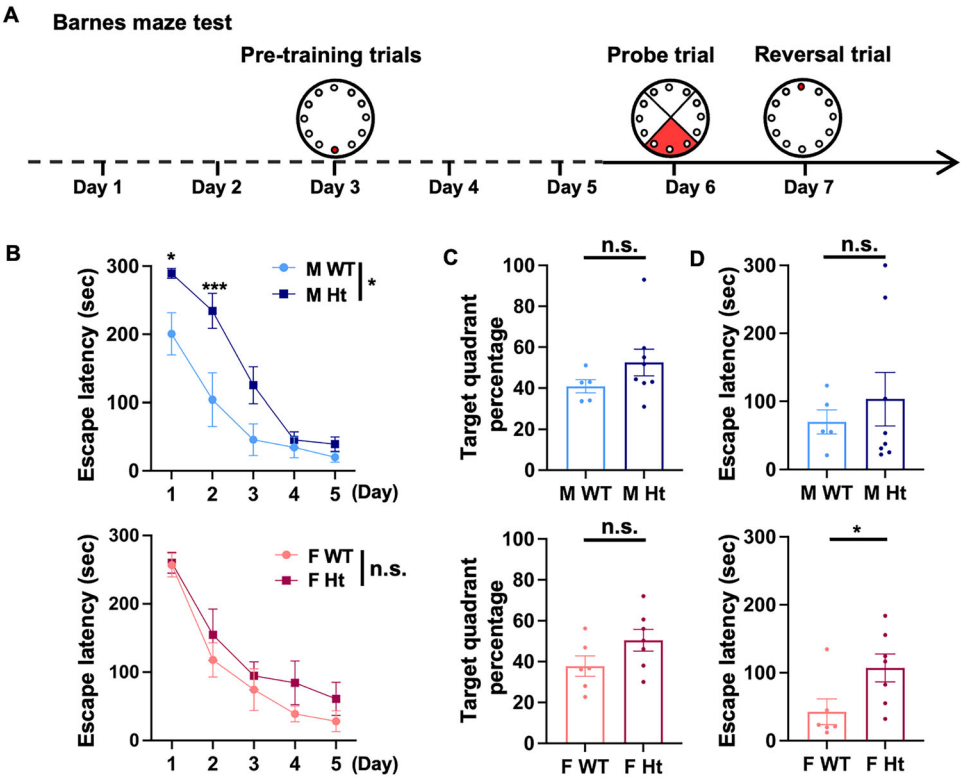

Fig. 4 CaMKIIα P212L Ht mice show impaired spatial learning in the Barnes maze test. A Experimental schedule for the Barnes maze test. After 5 days of pre-training, mice underwent a probe trial on the sixth day. The reversal trial was conducted after 24 h of the probe trial. **B** Average escape latency (4 trials per day) for 5 days (two-way repeated measures ANOVA test, Šídák post hoc test). **C** Percentage of time at target quadrant in the probe trial (unpaired Student's t-test). **D** Cognitive flexibility is impaired in CaMKIIα P212L female mice in the reversal trial (unpaired Student's t-test). Male: WT, n = 5. Ht, n = 8. Female: WT, n = 6. Ht, n = 7. Data represent mean ± SEM. *$p < 0.05$, ***$p < 0.001$.

mice. Furthermore, male Ht mice displayed exaggerated hippocampal LTP in response to a subthreshold low-frequency stimulation. At the behavior level, our model showed face validity, by exhibiting abnormalities in social behavior, motor coordination, anxiety- and fear-related behavior, and spatial and visually guided learning in male mice. Taken together, we propose that aberrant enhancement of CaMKIIα signaling by a heterozygous P212L mutation underlies the complex clinical phonotypes observed in a subset of ID/NDD features. Interestingly, the phenotypic traits of female Ht mice differed from those of males, suggesting sexual dimorphism is evident for CaMKIIα P212L mutations. We believe this novel mouse model is critical for furthering our understanding of the in vivo pathophysiology for ID/NDD traits arising from dysregulated CaMKII signaling.

Despite strong clinical genetic evidence for the possible causative impact of CaMKII mutations for ID [11–14], our ability to study these conditions is hampered by a lack of mouse models harboring such mutations. While there are previous studies with mouse models reflecting the ID patient-identified *CAMK2* de novo variants [39, 40], whether these mutations are causative for learning abnormalities has yet to be confirmed. Furthermore, in these studies, the behavioral phenotypes in heterozygous mice were mild or not significantly different from WT mice in these studies [39, 40], although the patients were reported to possess the heterozygous mutation. In contrast, our findings show that heterozygous CaMKIIα P212L knock-in mice display learning disabilities linked to ID in humans, ensuring construct and face validity reflecting the patient-derived de novo heterozygous variant of *CAMK2A*. CaMKIIα P212L is more frequent than other ID-associated mutations in CaMKIIα, and, this variant enhances Ca^{2+}/CaM-dependent activation, a molecular feature common to other ID-associated de novo *CAMK2A* mutants [13], this animal model can serve as a representative preclinical model for these de novo mutations.

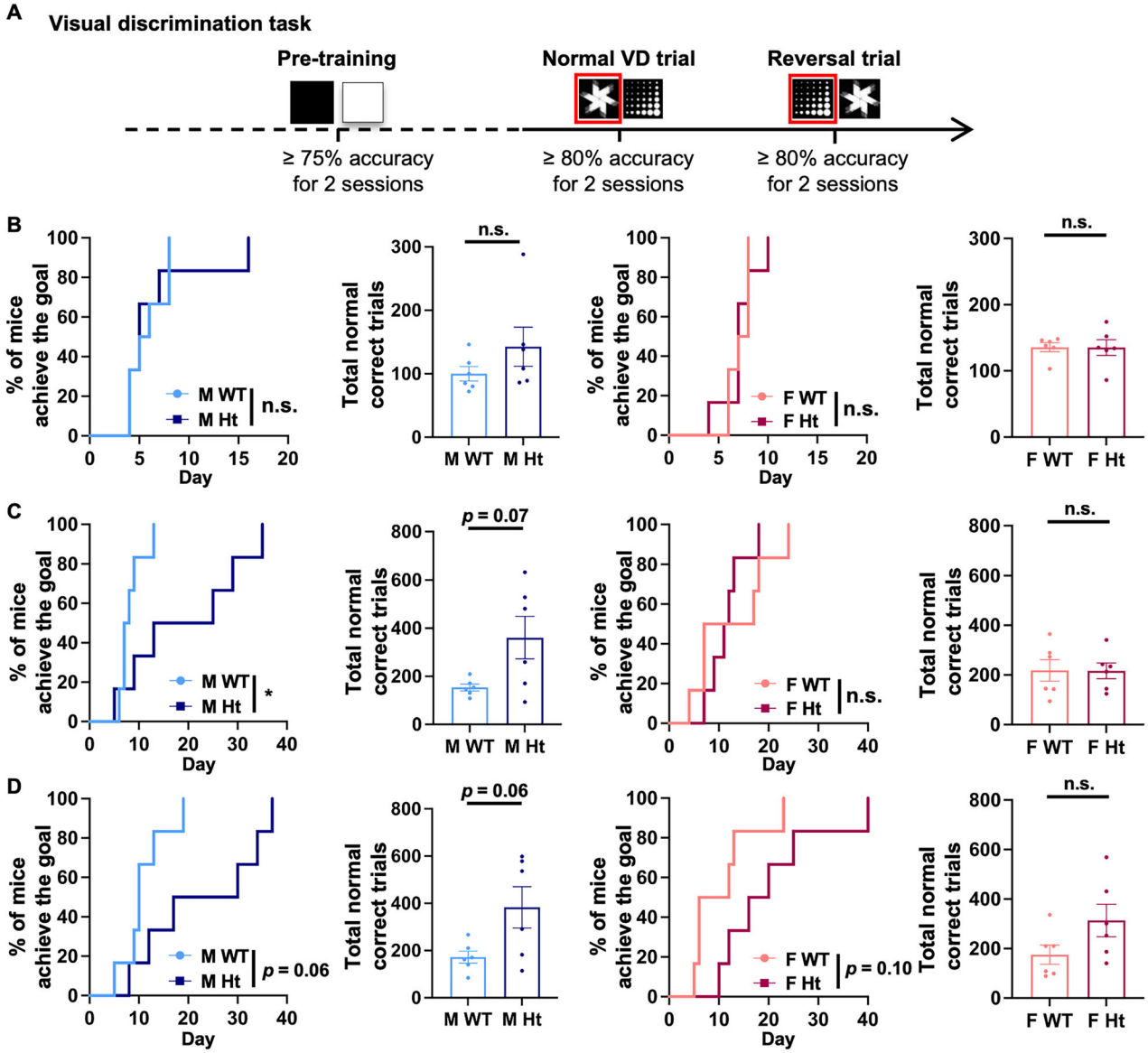

Fig. 5 Visually guided learning and memory are impaired in male CaMKIIα P212L Ht mice. A Experimental schedule for touchscreen-based behavioral tests. Mice achieved a performance level of ≥75% correct responses for 2 consecutive days in the pre-training trial before being subjected to the normal VD trial. Mice achieved a performance level of ≥80% correct responses for 2 consecutive days before being subjected to the reversal trial. **B** The percentage of mice that reached the learning criterion (Log-rank test) and total normal correct trials required (unpaired Student's t-test) in the pre-training session. **C** The percentage of mice that reached the learning criterion (Log-rank test) and total normal correct trials required (unpaired Student's t-test) in the normal VD trial. **D** Percentage of mice reach the learning criterion (Log-rank test) and total normal correct trials required (unpaired Student's t-test) in the reversal trial. Male: WT; n = 6, Ht; n = 6, Female: WT; n = 6. Ht; n = 6. Data represent mean ± SEM. *$p < 0.05$.

The CaMKIIα P212L Ht mice exhibited abnormal social behaviors, impaired motor coordination, enhanced anxiety- and fear-related behaviors, and diminished spatial and visually guided learning, mirroring the clinical diagnoses of the patients (ASD, DCD and ID). We found evidence for enhanced social interaction in CaMKIIα P212L Ht mice. Of note, applying the classical classification by Wing et al., which categorizes ASD into three subtypes——"aloof", "passive", and "active but odd" ——our patient carrying the CaMKIIα P212L variant was identified within the "active but odd" category [41]. This subgroup is characterized by active social approaches that are odd, inappropriate, and one-sided, which is consistent with the hypersocial behavior observed in our mouse model.

In some behavioral tests, female Ht mice exhibited phenotypes similar to male mice despite the absence of detectable biochemical changes. Interestingly, only male Ht mice showed elevated levels of relative T286 autophosphorylation of CaMKIIα in synaptosomes. This sex-dependent difference may be attributed to variations in synaptic molecular architecture influenced by sex hormones [42], suggesting that females employ mechanisms distinct from males to maintain synaptic signaling, potentially compensating for the genetic mutation of CaMKIIα under basal synaptic activity. The precise nature of these sex differences remains poorly understood, underscoring the need for further investigation. The discrepancy between our biochemical findings and behavioral results observed in female Ht mice may arise, at least in part, from the following experimental limitations. First, the biochemical experiments utilized whole brains from mice housed in home cages without external stimulation, which may have limited the detection of changes occurring in response to specific

stimuli or during certain time windows relevant to behavioral analyses. For instance, during fear-conditioning experiments, the conditioned and unconditioned stimulus are likely to induce robust synaptic transmission, potentially activating CaMKII in relevant brain regions such as the amygdala and the hippocampus. Given the Ca^{2+}-dependent activation property of CaMKII, it is plausible that these factors dynamically influence the levels of its autophosphorylation in a region-specific manner, differentially between WT and Ht mice, but the changes may remain undetectable under our experimental conditions. Second, considering the critical role of CaMKII during neuronal development [43, 44], it is possible that the mutation affects neural circuit architecture, contributing to behavioral control in ways that may not be fully captured through biochemical analyses. The specific mechanisms through which CaMKIIα P212L mutation affects each behavioral phenotype require further exploration.

Through the Barnes maze and VD tests for spatial and visually guided learning and memory, respectively, we found that only male P212L Ht mice exhibited a significant learning delay, whereas female Ht mice showed impaired cognitive flexibility in a reversal trial in the Barnes maze. Such differences could reflect sexual dimorphism for learning and memory. For example, male rodents have been found to rely on a hippocampus-dependent place strategy rather than a striatum-dependent response strategy for learning, while female rodents exhibit a preference for a place strategy only when estradiol levels are elevated [45]. Furthermore, cognitive flexibility is influenced by the estrous cycle and stress conditions in a sex-dependent manner, with stress negatively impacting it in female rodents [46]. One possible reason for the impaired cognitive flexibility only in female Ht mice is that the behavioral task itself imposed stress, potentially affecting their cognitive flexibility. Although the mechanisms behind this multi-scale sexual dimorphism are still unclear, our findings align with current evidence showing that males with the P212L mutation have more severe ID phenotypes and co-morbid seizures compared to females (Table 1). However, this should be clarified from more patients in the future, as reports of patients with the P212L mutation remain very limited [11, 13], with only four cases documented to date restricting the available information. Our findings are also consistent with epidemiological studies indicating a higher prevalence of ID in males compared to females [47]. Consistently, sex differences have been observed in model mice of other NDD-related synaptic genes, such as *GABRB3* and *NRXN1* [48]. The mechanisms underlying these differences are not fully understood, but it is likely that sex hormones, the age at testing, compensatory mechanisms, and the complex effects of these genetic mutations on brain structure and function collectively influence the phenotypic variability [48].

Hippocampal LTP is recognized as a key mechanism that underlies learning and memory, and CaMKII has been proven to be a central player in LTP regulation [7–10]. We found that male CaMKIIα P212L Ht mice showed a significant LTP after low-frequency stimulation (10 Hz, 90 s), a frequency that does not induce potent plasticity in WT animals. This finding is consistent with our previous study using a FRET sensor, in which we demonstrated that CaMKIIα P212L conferred facilitated Ca^{2+}/CaM-dependent activation [13]. Notably, several mutant mice have been developed to encode mutations to CaMKIIα that likely increase enzymatic activity: T286D (a phospho-mimic mutation inducing autonomous activity) [49, 50] and T305V/T306A (phospho-deficient mutations at inhibitory phosphorylation sites) [24, 51]. These mutant mice exhibited excessive LTP at low-frequency stimulation and various degrees of deficits in learning and memory, a finding consistent with our present findings. Since the P212L mutation exhibited lower frequency-tuning for its kinase activation, we propose that low-frequency stimulation of the hippocampus is sufficient to activate CaMKIIα P212L, leading to mistuning of synaptic plasticity, and resulting in learning and memory deficits, which may cause phenotypes related to ID.

Many synaptic and/or Ca^{2+} signaling genes, such as *GRINs*, *SYNGAP1*, and *SHANK3*, are identified as risk genes for ID [52–54] and other NDDs. Despite the availability of these animal models, the precise pathological mechanisms underlying ID and effective treatment methods remain elusive. In this study, we have established a CaMKIIα P212L mouse model with construct and face validity. Given that CaMKIIα is an essential synaptic and calcium-dependent signaling mediator governing learning and memory and acts as a critical hub molecule linking these other ID-related genes, its enzymatic dysregulation may also underlie the pathogenesis of different forms of ID/NDDs, including those induced by mutations in other synaptic genes. Thus, our mouse model will be important for further understanding ID/NDDs arising from CaMKII dysregulations and offering perspectives for future therapeutic strategies.

DATA AVAILABILITY

The datasets generated and/or analyzed during this study are available from the corresponding author upon reasonable request.

REFERENCES

1. American Psychiatric Association. Diagnostic and Statistical Manual of Mental Disorders. American Psychiatric Pub. United States, 2013.
2. Morris-Rosendahl DJ, Crocq M-A. Neurodevelopmental disorders-the history and future of a diagnostic concept. Dialogues Clin Neurosci. 2020;22:65–72.
3. Gilissen C, Hehir-Kwa JY, Thung DT, van de Vorst M, van Bon BWM, Willemsen MH, et al. Genome sequencing identifies major causes of severe intellectual disability. Nature. 2014;511:344–7.
4. Vissers LELM, Gilissen C, Veltman JA. Genetic studies in intellectual disability and related disorders. Nat Rev Genet. 2016;17:9–18.
5. Yasuda R, Hayashi Y, Hell JW. CaMKII: a central molecular organizer of synaptic plasticity, learning and memory. Nat Rev Neurosci. 2022;23:666–82.
6. Nicoll RA, Schulman H. Synaptic memory and CaMKII. Physiol Rev. 2023;103:2877–925.
7. Lisman J, Malenka RC, Nicoll RA, Malinow R. Learning mechanisms: the case for CaM-KII. Science. 1997;276:2001–2.
8. Lisman J, Yasuda R, Raghavachari S. Mechanisms of CaMKII action in long-term potentiation. Nat Rev Neurosci. 2012;13:169–82.
9. Takemoto-Kimura S, Suzuki K, Horigane S, Kamijo S, Inoue M, Sakamoto M, et al. Calmodulin kinases: essential regulators in health and disease. J Neurochem. 2017;141:808–18.
10. Bayer KU, Schulman H. CaM kinase: still inspiring at 40. Neuron. 2019;103:380–94.
11. Küry S, Van Woerden GM, Besnard T, Proietti Onori M, Latypova X, Towne MC, et al. De novo mutations in protein kinase genes CAMK2A and CAMK2B cause intellectual disability. Am J Hum Genet. 2017;101:768–88.
12. Akita T, Aoto K, Kato M, Shiina M, Mutoh H, Nakashima M, et al. De novo variants in CAMK2A and CAMK2B cause neurodevelopmental disorders. Ann Clin Transl Neurol. 2018;5:280–96.
13. Fujii H, Kidokoro H, Kondo Y, Kawaguchi M, Horigane S, Natsume J, et al. Förster resonance energy transfer-based kinase mutation phenotyping reveals an aberrant facilitation of Ca^{2+}/calmodulin-dependent CaMKIIα activity in de novo mutations related to intellectual disability. Front Mol Neurosci. 2022;15:970031.
14. Chia PH, Zhong FL, Niwa S, Bonnard C, Utami KH, Zeng R, et al. A homozygous loss-of-function CAMK2A mutation causes growth delay, frequent seizures and severe intellectual disability. eLife. 2018;7:e32451.
15. Hudmon A, Schulman H. Neuronal CA^{2+}/calmodulin-dependent protein kinase II: the role of structure and autoregulation in cellular function. Annu Rev Biochem. 2002;71:473–510.
16. Tullis JE, Larsen ME, Rumian NL, Freund RK, Boxer EE, Brown CN, et al. LTP induction by structural rather than enzymatic functions of CaMKII. Nature. 2023;621:146–53.
17. Chen X, Cai Q, Zhou J, Pleasure SJ, Schulman H, Zhang M, et al. CaMKII autophosphorylation is the only enzymatic event required for synaptic memory. Proc Natl Acad Sci USA. 2024;121:e2402783121.
18. Liu P-W, Hosokawa T, Hayashi Y. Regulation of synaptic nanodomain by liquid-liquid phase separation: a novel mechanism of synaptic plasticity. Curr Opin Neurobiol. 2021;69:84–92.
19. Silva AJ, Stevens CF, Tonegawa S, Wang Y. Deficient hippocampal long-term potentiation in α-calcium-calmodulin kinase II mutant mice. Science. 1992;257:201–6.
20. Silva AJ, Paylor R, Wehner JM, Tonegawa S. Impaired spatial learning in α-calcium-calmodulin kinase II mutant mice. Science. 1992;257:206–11.
21. Mayford M, Wang J, Kandel ER, O'Dell TJ. CaMKII regulates the frequency-response function of hippocampal synapses for the production of both LTD and LTP. Cell. 1995;81:891–904.

22. Bach ME, Hawkins RD, Osman M, Kandel ER, Mayford M. Impairment of spatial but not contextual memory in CaMKII mutant mice with a selective loss of hippocampal LTP in the range of the theta frequency. Cell. 1995;81:905–15.
23. Giese KP, Fedorov NB, Filipkowski RK, Silva AJ. Autophosphorylation at Thr286 of the alpha calcium-calmodulin kinase II in LTP and learning. Science. 1998;279:870–3.
24. Elgersma Y, Fedorov NB, Ikonen S, Choi ES, Elgersma M, Carvalho OM, et al. Inhibitory autophosphorylation of CaMKII controls PSD Association, plasticity, and learning. Neuron. 2002;36:493–505.
25. De Koninck P, Schulman H. Sensitivity of CaM kinase II to the frequency of Ca^{2+} oscillations. Science. 1998;279:227–30.
26. Fujii H, Inoue M, Okuno H, Sano Y, Takemoto-Kimura S, Kitamura K, et al. Nonlinear decoding and asymmetric representation of neuronal input information by CaMKIIα and calcineurin. Cell Rep. 2013;3:978–87.
27. Fujii H, Bito H. Deciphering Ca^{2+}-controlled biochemical computation governing neural circuit dynamics via multiplex imaging. Neurosci Res. 2022;179:79–90.
28. Sawahata M, Mori D, Arioka Y, Kubo H, Kushima I, Kitagawa K, et al. Generation and analysis of novel Reln-deleted mouse model corresponding to exonic Reln deletion in schizophrenia. Psychiatry Clin Neurosci. 2020;74:318–27.
29. Massaro Tieze S, Chandra SS, Vidyadhara DJ. Subcellular fractionation for the isolation of synaptic components from the murine brain. J Vis Exp. 2022. https://doi.org/10.3791/64574.
30. Schulman H, Greengard P. Stimulation of brain membrane protein phosphorylation by calcium and an endogenous heat-stable protein. Nature. 1978;271:478–9.
31. Konno A, Hirai H. Efficient whole brain transduction by systemic infusion of minimally purified AAV-PHP.eB. J Neurosci Methods. 2020;346:108914.
32. Kim J-Y, Grunke SD, Levites Y, Golde TE, Jankowsky JL Intracerebroventricular viral injection of the neonatal mouse brain for persistent and widespread neuronal transduction. J Vis Exp. 2014:51863. https://doi.org/10.3791/51863.
33. Sobue A, Ito N, Nagai T, Shan W, Hada K, Nakajima A, et al. Astroglial major histocompatibility complex class I following immune activation leads to behavioral and neuropathological changes. Glia. 2018;66:1034–52.
34. Ueda S, Hosokawa M, Arikawa K, Takahashi K, Fujiwara M, Kakita M, et al. Distinctive regulation of emotional behaviors and fear-related gene expression responses in two extended amygdala subnuclei with similar molecular profiles. Front Mol Neurosci. 2021;14:741895.
35. Bussey TJ, Padain TL, Skillings EA, Winters BD, Morton AJ, Saksida LM. The touchscreen cognitive testing method for rodents: how to get the best out of your rat. Learn Mem. 2008;15:516–23.
36. Horner AE, Heath CJ, Hvoslef-Eide M, Kent BA, Kim CH, Nilsson SRO, et al. The touchscreen operant platform for testing learning and memory in rats and mice. Nat Protoc. 2013;8:1961–84.
37. Liao J, Dong G, Wulaer B, Sawahata M, Mizoguchi H, Mori D, et al. Mice with exonic RELN deletion identified from a patient with schizophrenia have impaired visual discrimination learning and reversal learning in touchscreen operant tasks. Behav Brain Res. 2022;416:113569.
38. Mutoh H, Aoto K, Miyazaki T, Fukuda A, Saitsu H. Elucidation of pathological mechanism caused by human disease mutation in CaMKIIβ. J Neurosci Res. 2022;100:880–96.
39. Stephenson JR, Wang X, Perfitt TL, Parrish WP, Shonesy BC, Marks CR, et al. A novel human CAMK2A mutation disrupts dendritic morphology and synaptic transmission, and causes ASD-related behaviors. J Neurosci. 2017;37:2216–33.
40. Pi HJ, Otmakhov N, El Gaamouch F, Lemelin D, De Koninck P, Lisman J. CaMKII control of spine size and synaptic strength: role of phosphorylation states and nonenzymatic action. Proc Natl Acad Sci USA. 2010;107:14437–42.
41. Wing L. The autistic spectrum. Lancet. 1997;350:1761–6.
42. Uhl M, Schmeisser MJ, Schumann S. The sexual dimorphic synapse: from spine. density to molecular composition. Front Mol Neurosci. 2022;15:818390.
43. Wayman GA, Lee Y-S, Tokumitsu H, Silva AJ, Soderling TR. Calmodulin-kinases: modulators of neuronal development and plasticity. Neuron. 2008;59:914–31.
44. Takemoto-Kimura S, Suzuki K, Kamijo S, Ageta-Ishihara N, Fujii H, Okuno H, et al. Differential roles for CaM kinases in mediating excitation-morphogenesis coupling during formation and maturation of neuronal circuits. Eur J Neurosci. 2010;32:224–30.
45. Hawley WR, Grissom EM, Barratt HE, Conrad TS, Dohanich GP. The effects of biological sex and gonadal hormones on learning strategy in adult rats. Physiol Behav. 2012;105:1014–20.
46. Koszałka A, Lustyk K, Pytka K. Sex-dependent differences in animal cognition. Neurosci Biobehav Rev. 2023;153:105374.
47. Bölte S, Neufeld J, Marschik PB, Williams ZJ, Gallagher L, Lai M-C. Sex and gender in neurodevelopmental conditions. Nat Rev Neurol. 2023;19:136–59.
48. Mossa A, Manzini MC. Molecular causes of sex-specific deficits in rodent models of. neurodevelopmental disorders. J Neurosci Res. 2021;99:37–56.
49. Mayford M, Bach ME, Huang YY, Wang L, Hawkins RD, Kandel ER. Control of memory formation through regulated expression of a CaMKII transgene. Science. 1996;274:1678–83.
50. Bejar R, Yasuda R, Krugers H, Hood K, Mayford M. Transgenic calmodulin-dependent protein kinase II activation: dose-dependent effects on synaptic plasticity, learning, and memory. J Neurosci. 2002;22:5719–26.
51. Chang J-Y, Nakahata Y, Hayano Y, Yasuda R. Mechanisms of Ca^{2+}/calmodulin-dependent kinase II activation in single dendritic spines. Nat Commun. 2019;10:2784.
52. Holder JL, Hamdan FF, Michaud JL. SYNGAP1-related intellectual disability. In: Adam MP, Feldman J, Mirzaa GM, Pagon RA, Wallace SE, Bean LJ, et al., editors. GeneReviews®, Seattle (WA): University of Washington, Seattle; 2019.
53. Bruno LP, Doddato G, Valentino F, Baldassarri M, Tita R, Fallerini C, et al. New candidates for autism/intellectual disability identified by whole-exome sequencing. Int J Mol Sci. 2021;22:13439.
54. Platzer K, Lemke JR GRIN1-related neurodevelopmental disorder. In: Adam MP, Feldman J, Mirzaa GM, Pagon RA, Wallace SE, Bean LJ, et al., editors. GeneReviews®, Seattle (WA): University of Washington, Seattle; 2019.

ACKNOWLEDGEMENTS

We thank all members of the Takemoto laboratory for support and discussion, and the Center for Animal Research and Education (CARE) at Nagoya University for technical support for animal experiments. This work was supported in part by JSPS KAKENHI JP24K10490, JP22K15638 (SH), JP20H03339, JP23H02795, JP23K27486, JP23K17639 (ST-K), JP22H03542, JP21K18564 (AMW), JP22K06454, JP24H01221(AK); AMED SICORP 23jm0210098 (HB); AMED Brain/MINDS JP19dm0207081 (AMW), JP21dm0207111 (HH); AMED Brain/MINDS 2.0 JP24wm0625103 (HH); JST (Moonshot R and D) JPMJMS2024 (AMW); Toyoaki Scholarship Foundation (ST-K, DM); The Kawano Masanori Memorial Public Interest Incorporated Foundation for Promotion of Pediatrics (ST-K); the Daiko Foundation (ST-K, P-WL); The Japan Foundation for Applied Enzymology (ST-K); Brain Science Foundation (ST-K); Kobayashi Foundation (ST-K). MP is supported by a scholarship from China Scholarship Council (CSC) for PhD program. We also thank Dr. Julian Heng (ORCID: 0000-0002-0378-7078) provided professional English-language editing of this article (Certificate No. 4Eg5Ec5P).

AUTHOR CONTRIBUTIONS

MP, P-WL, and ST-K designed the research; MP, P-WL, YO, FA-Y, GD, MS, DM, MN, YY, XL, HN, SH performed the research; AK, HH contributed new reagents/analytic tools; HF, SU, NO, KY, HK, HB, HM, AMW, SH, ST-K supervised the projects; MP, P-WL, YO, SH, ST-K wrote the paper with input from all authors.

COMPETING INTERESTS

The authors declare no competing interests.

ADDITIONAL INFORMATION

Supplementary information The online version contains supplementary material available at https://doi.org/10.1038/s41398-025-03316-4.

Correspondence and requests for materials should be addressed to Sayaka Takemoto-Kimura.